Available online at www.sciencedirect.com
SCIENCE DIRECT®
Journal of Nuclear Materials 325 (2004) 44–52
journal of nuclear materials
www.elsevier.com/locate/jnucmat

Master equation and Fokker–Planck methods for void nucleation and growth in irradiation swelling

M.P. Surh, J.B. Sturgeon *, W.G. Wolfer

Lawrence Livermore National Laboratory, Livermore, L-353, P.O. Box 808, California 94550, USA

Received 30 June 2003; accepted 30 October 2003

Abstract

A complete theory of void swelling in irradiated metals requires the treatment of defect cluster nucleation events, as well as subsequent growth of stable clusters. One difficulty is that small-voids evolve rapidly and reversibly, whereas the secular evolution of the overall system is extremely slow. Thus, rate theory models for the void size distribution entail a set of stiff, coupled equations. A combined Master equation and Fokker–Planck numerical approach is introduced to address this problem and permit large time-steps at late times. Calculations are stable in practice, easily converged, and computationally efficient to large doses over a wide range in temperatures. The results are encouraging compared to experiment and earlier, related calculations.

1. Introduction

Void swelling is an important consideration for long-term materials reliability in a radiation environment. Careful studies of a temperature- and flux-dependent transient delay to swelling suggest that the initial microstructural evolution may determine the ultimate material longevity. This 'incubation' stage often persists for tens of displacements per atom (dpa) of irradiation, during which little swelling occurs. Once stable voids finally accumulate, they can rapidly grow larger under irradiation. This causes secular changes detrimental to material properties, e.g., volume increases of 1% per dpa in austenitic stainless steel [1–5]. Such rapid swelling can quickly render a material unusable for engineering applications.

Irradiation damage alters microstructure in several ways. It directly creates residual atomic defects and small defect clusters, it slowly modifies the pre-existing dislocation network and impurity distribution, and it gradually introduces new impurities by nuclear transmutation and decay. Small defect clusters are often impermanent, annihilating, dissociating, being absorbed at dislocations or grain boundaries, or being engulfed by later damage cascades. Thus, the population of small defect clusters quickly reaches a quasi-stationary distribution [6]. In the absence of permanent vacancy clusters, interstitial- and vacancy-type defects are absorbed at dislocations in equal amounts, and there is no further volume change on average. Rarely, a stable void nucleates and grows larger under the radiation-induced vacancy supersaturation. When such cavities exist in significant numbers, swelling becomes a segregation process, with interstitials preferentially absorbing at dislocations and vacancies at voids [7].

It is evident from transmission electron microscopy that stable void nucleation occurs transiently. The total measured density of large voids is essentially constant during the late-stage, steady swelling, so no new voids are being created at these times [8]. This is as expected, since the theoretical rate of void nucleation is exponentially sensitive to the vacancy supersaturation [9,10]. Stable voids act as vacancy sinks, depleting the radiation-driven supersaturation and preventing the nucleation of additional voids. This sensitivity also implies that the total void nucleation time will depend on

* Corresponding author.
E-mail address: sturgeon2@llnl.gov (J.B. Sturgeon).

0022-3115/$ - see front matter © 2003 Elsevier B.V. All rights reserved.
doi:10.1016/j.jnucmat.2003.10.013

temperature and irradiation dose rate. Together, these characteristics suggest that void nucleation is a necessary pre-cursor to steady swelling and may be the proximate cause of the temperature- and dose-rate-dependent incubation delay.

We have developed a computational approach for treating void nucleation and growth in detail that evaluates the density of vacancy clusters of all sizes from monomers to arbitrary sizes. In this approach, the time-dependent state of a high-purity metal under irradiation is described by the thermodynamic parameters of temperature and pressure, the non-equilibrium, mobile point defect concentrations (irradiation cascade-induced monomer vacancies, C_v, and interstitials, C_i) and the densities of extended defects. (The defect distribution function, ρ, is currently limited to voids and network dislocations, $\rho = \rho_{void} + \rho_{disl}$.) The irradiation damage is introduced as isolated monomers rather than as a statistical distribution of ready-made defect clusters [11–16]. Spatial relations between cluster defects are neglected, in effect assuming that the void density is low, pre-existing material inhomogeneity is insignificant, and spatial pattern formation does not occur in the defect densities. Thus, the present approach does not account for grain boundaries or dislocation cell walls. There is similarly no coalescence or impingement of voids on each other or on dislocations.

Once created, mobile point defects diffuse under the influence of stress-mediated interactions and annihilate or are absorbed at defect sinks. These sinks include vacancy clusters and dislocations. The radiation damage thereby feeds simultaneously the climb of dislocations and growth of voids. We treat this reaction-diffusion problem by mean field approximation [17,18]. The (sessile) voids evolve by a series of coupled reactions with monomer defects, e.g., vacancy monomer plus n-vacancy cluster in a reversible reaction, $v + v_n \Longleftrightarrow v_{n+1}$, etc., or irreversible interstitial reactions, $i + v_n \rightarrow v_{n-1}$. In turn, the instantaneous monomer densities are coupled to the population of larger defects (monomer sinks/sources). This self-consistent feedback causes the rates of void growth and size-fluctuation to be time-dependent functionals of the entire void distribution and dislocation density, as well as the temperature and irradiation rate. For example, the calculation automatically suppresses void nucleation as the vacancy supersaturation evolves in time or as the competition for vacancy capture at the various sinks changes.

We decouple this system of non-linear reaction equations to evaluate the evolution [10]. First, the time-dependent monomer concentrations are obtained analytically from coupled, quadratic rate equations. Their solution assumes a quasi-stationary monomer concentration appropriate to the instantaneous density of monomer sinks/sources (i.e. voids and dislocations), essentially as in Ref. [10]. The population of clusters of all kinds, s, is held constant at instantaneous values, $\rho(s,t)$, when solving these equations. Subsequently, the void distribution function, ρ_{void}, is incrementally evolved in time while holding the monomer concentrations fixed, effectively linearizing the binary monomer-void reaction rate equations over short-time intervals. It is useful to enforce mass balance between these two steps to ensure the accuracy of the final swelling results. That is, for every vacancy created there is a compensating interstitial so the number of atoms remains always conserved. As a result, the vacancy rate equation is more elaborate here than in earlier implementations [10,19].

The coupled monomer rate equations are:

$$\begin{aligned} 0 &\cong \frac{dC_v}{dt} \\ &= P_v - \kappa D_v C_v(t) D_i C_i(t) - D_v C_v(t) \overline{Z}_v \overline{S} \\ &\quad + D_i C_i(t) \rho(v_2,t) Z_i(v_2) A(v_2) + D_v \overline{C_v^{evap}} \overline{Z}_v \overline{S}, \end{aligned} \tag{1}$$

$$\begin{aligned} 0 &\cong \frac{dC_i}{dt} \\ &= P_i - \kappa D_v C_v(t) D_i C_i(t) - D_i C_i(t) \overline{Z}_i \overline{S} \\ &\quad + D_i C_i(t) \rho(v_2,t) Z_i(v_2) A(v_2), \end{aligned} \tag{2}$$

in the quasi-stationary limit, where C are the instantaneous monomer concentrations to be solved, D are their diffusivities, and P are the radiation-induced monomer production rates per unit volume, v denotes the vacancy monomer, v_n denotes the n-vacancy cluster, and i denotes the interstitial monomer. Vacancy and interstitial production rates are taken to be equal, $P_i = P_v$. The second term in both equations, $\kappa D_v C_v D_i C_i$, describes the rate of direct vacancy-interstitial annihilation. Monomer absorption at all other defects, s, is included by the third term with aggregate parameters:

$$\overline{S} = \sum_s \rho(s,t) A(s), \tag{3}$$

$$\overline{Z}_i \overline{S} = \sum_s \rho(s,t) Z_i(s) A(s) + \rho(v_2,t) Z_i(v_2) A(v_2), \tag{4}$$

$$\overline{Z}_v \overline{S} = \sum_s \rho(s,t) Z_v(s) A(s) + 2\rho(v,t) Z_i(v) A(v), \tag{5}$$

where $\rho(s,t)$ is the concentration of sinks of type s; A are cross-sections for monomer impingement; and bias factors, Z, for interstitials or vacancies quantify the effects of long-range interactions between sinks and monomers [17,18] on impingement rates. The cross-section and bias factors simply parametrize the mean-field solution for the flux of mobile monomers to the sinks. (Here, s denotes all of the composite defects, i.e., dislocations and voids, including vacancy dimers and larger clusters. The monomer rate equation depends explicitly (i.e. the

solution to the next time-step depends on quantities from the previous one) on these aggregate parameters, so that, e.g., $\frac{dC_v}{dt}|_{t+\tau}$ at time $t+\tau$ depends on the cluster parameters at time t. This explicit coupling demands an appropriately short time-step, t, which is established in practice by seeking stable, well-converged results.)

The rate of vacancy–vacancy aggregation, $v+v \rightarrow v_2$, is given by the second term in the expression for $\overline{Z_v}$, in terms of the vacancy–vacancy cross-sections, A_v, and bias factors, $Z_v(v)$. The factor of 2 in this term indicates that the process removes two vacancies from the population. (The relative mobility of the pair is given by $2D_v$, but the reaction rate coefficient must be corrected by 1/2 to avoid double-counting pairs of monomers.) All composite defects (vacancy clusters and dislocations) are also assumed to have negligible diffusivity compared to the monomers. The last term in the vacancy rate equation describes the thermal emission of vacancies by dislocations and voids.

$$\overline{C_v^{\mathrm{evap}}}\overline{Z}_v\overline{S} = \sum_s \rho(s,t)Z_v(s-v)A(s-v)C_v^{\mathrm{eq}}(s,t) + \rho(v_2,t)Z_v(v)A(v)C_v^{\mathrm{eq}}(v_2,t), \tag{6}$$

given in terms of the equilibrium vacancy concentration for each particular defect cluster. The cross-sections and bias factors that are employed here are appropriate to the defect minus one vacancy, as required by detailed balance. The summation is augmented by an extra contribution from $v_2 \rightarrow v+v$, thereby counting the dimer dissociation process twice, in accordance with its production of two vacancies. Finally, the fourth term in the vacancy rate equation describes the annihilation of an interstitial at a vacancy dimer, $i+v_2 \rightarrow v$, which yields one vacancy. The interstitial equation has been written to include the same term, by defining $\overline{Z}_i$ appropriately. The actual aggregate interstitial sink strength is given by:

$$\widetilde{Z}_i\overline{S} = \overline{Z}_i\overline{S} - \rho(v_2,t)Z_i(v_2)A(v_2). \tag{7}$$

The analytic solution to these coupled quadratic equations is:

$$D_iC_i = \frac{1}{2}\left(\sqrt{L^2+M}-L\right), \tag{8}$$

$$L = \frac{(P_v-P_i)}{\overline{S}\overline{Z}_i} + \frac{\overline{Z}_v}{\overline{Z}_i}D_v\overline{C_v^{\mathrm{evap}}} + \overline{Z}_v\overline{S}\frac{\widetilde{Z}_i}{\overline{Z}_i}\times\frac{1}{\kappa}, \tag{9}$$

$$M = 4P_i\frac{\overline{Z}_v}{\overline{Z}_i}\times\frac{1}{\kappa}, \tag{10}$$

$$D_vC_v = \frac{\overline{Z}_i}{\overline{Z}_v}D_iC_i - \frac{(P_i-P_v)}{\overline{S}\overline{Z}_v} + D_v\overline{C_v^{\mathrm{evap}}}. \tag{11}$$

In practical implementations, $C_v(t+\tau)$ is obtained from these equations in terms of $\rho(t)$ from the previous iteration. The vacancy concentration appears in two places, as the unknown C_v and as a portion of the sink terms, as $\rho(v,t)$. These quantities should be equal. Accordingly, we solve the equations iteratively in order to obtain $\rho(v,t+\tau)$. All other cluster densities continue to be specified at time t. Self-consistency seems to improve the mass-conservation, besides eliminating a minor inconsistency, and the added computational effort is small.

The second step in the numerical time evolution updates the void size distribution function under the flux of mobile vacancies and interstitials. (The dislocation subsystem is described by a single, time-independent density parameter, ρ_{disl}, in the present approach.) The distribution function, $\rho(v_n,t) = \rho_{\mathrm{void}}(n,t)$, expresses the time-dependent density of voids of a given size, n, spanning the range from vacancy monomers to voids of arbitrary size. All voids are approximated as spherical in shape. The governing Master equation is specified by the rates at which voids add a vacancy, lose a vacancy to thermal emission, or lose a vacancy by absorbing an interstitial atom (at rates β, θ, α respectively [10]). These are identical to the sink terms in the monomer rate equations, i.e., for a cluster of n-vacancies:

$$\alpha(v_n,t) = D_iC_i(t)A(v_n)Z_v(v_n), \tag{12}$$

$$\beta(v_n,t) = D_vC_v(t)A(v_n)Z_v(v_n), \tag{13}$$

$$\theta(v_n) = D_vC_v^{\mathrm{eq}}(v_n)A(v_{n-1})Z_v(v_{n-1}), \tag{14}$$

where the concentrations C_v and C_i are held fixed at the values given by the monomer rate equation at time t.

The resulting equations are tridagonal in matrix form, and linear, $\frac{d\vec{\rho}}{dt} = \overline{M}\vec{\rho}$:

$$\rho(v) = C_v(t), \tag{15}$$

$$\frac{d\rho(v_2)}{dt} = [\beta(v)]\rho(v) - [\alpha(v_2)+\beta(v_2)+\theta(v_2)]\rho(v_2) + [\alpha(v_3)+\theta(v_3)]\rho(v_3), \tag{16}$$

$$\frac{d\rho(v_3)}{dt} = [\beta(v_2)]\rho(v_2) - [\alpha(v_3)+\beta(v_3)+\theta(v_3)]\rho(v_3) + [\alpha(v_4)+\theta(v_4)]\rho(v_4), \tag{17}$$

$$\vdots$$

$$\frac{d\rho(v_n)}{dt} = [\beta(v_{n-1})]\rho(v_{n-1}) - [\alpha(v_n)+\beta(v_n)+\theta(v_n)]\rho(v_n) + [\alpha(v_{n+1})+\theta(v_{n+1})]\rho(v_{n+1}), \tag{18}$$

where the vacancy monomer density is already obtained from the solution to the monomer rate equation, (i.e. the boundary condition at $n=1$ is specified by equating the monomer concentration to the solution of the monomer

rate equation, $\rho(v,t) \equiv C_v(t)$). The distribution is also zero as $n \to \infty$.

After updating the cluster distribution function, it is necessary to re-compute the monomer sink strengths and vacancy emission rates for the entire distribution of voids. This gives the sink/source terms for the next solution to the monomer equations. The procedure is iterated over successive intervals τ.

In practice, the net time-integrated flux of vacancies (minus interstitials) to the voids equates to the accumulated volume of those voids only when incremental changes, $\rho(t+\tau) - \rho(t)$, are linear in $\frac{d\rho}{dt}\tau$. (Equality between these two measures of swelling must be preserved in order to maintain mass-conservation.) The forwards Euler method of solution is linear, and gives a term-by-term cancellation between the quasi-stationary absorption/emission rates in the monomer equations and the net evolution of the clusters. Such an explicit solution is easily obtained. However, this conditionally convergent approach is unsatisfactory because it is restricted to small time-steps. Backwards Euler method would be stable, but it is a non-linear method. It includes higher-order terms in $\frac{d\rho}{dt}\tau$ that are not present in the monomer rate equations, so the overall system evolution does not strictly conserve mass.

Regardless of the method of solution, the Master equation approach becomes inefficient as the simulation progresses. The grid of integer void sizes, n, reaches from monomers to the largest cluster in the system, and the matrix problem grows to impractical size. At the same time, cluster densities between the large and small limits decrease to negligible levels, so that most of the size domain could be ignored. Euler methods also require that relative changes in the distribution be kept small over successive iterations [20]. As the stable clusters grow to larger size, the distribution is rapidly changing at the leading and trailing edges (Fig. 2). The rapid evolution at these transient edges confines the backwards Euler method to small values of τ [20].

We address these various difficulties by making a continuum approximation for the cluster sizes. The discrete Master equation is transformed to a Fokker–Planck equation for continuous size coordinate n:

$$\frac{\partial \rho^{\mathrm{FP}}(n,t)}{\partial t} = -\frac{\partial}{\partial n} K_{\mathrm{drift}}(n)\rho^{\mathrm{FP}}(n) + \frac{1}{2}\frac{\partial^2}{\partial n^2} Q_{\mathrm{diff}}(n)\rho^{\mathrm{FP}}(n). \tag{19}$$

The Fokker–Planck equation approximates the discrete evolution for size-dependent drift and diffusion coefficients:

$$K_{\mathrm{drift}}(n) = [\beta(n) - \alpha(n) - \theta(n)], \tag{20}$$

$$Q_{\mathrm{diff}}(n) = \frac{1}{2}[\alpha(n) + \beta(n) + \theta(n)]. \tag{21}$$

A path integral formalism has been applied to this equation before [10], where the short-time propagator is:

$$G(n,n',\tau) = \frac{1}{\sqrt{2\pi Q\tau}} \mathrm{e}^{-(n-n'-K\tau)^2/(2Q\tau)}. \tag{22}$$

This method is non-linear in τ, unconditionally stable, and conserves mass. A straightforward computational implementation still includes all sizes from smallest to largest, although it allows coarse-graining of the numerical grid.

Ultimately, however, it is preferable to solve the void evolution independent of any grid over size. Such a method would efficiently extend to multiple dimensions, where grid methods become computationally prohibitive. (Such extension permits the inclusion of helium and hydrogen content in addition to cavity size for future simulations of irradiation-induced void/bubble growth.) Accordingly, we employ a continuum, Langevin Monte Carlo scheme to model the size distribution function. When the number of Langevin particles, N, is large, their distribution approximates a continuous $\rho(n,t)$. A biased random-walk approximates the Fokker–Planck evolution. In our case, a 'particle' represents an ensemble (with a given density) of identical clusters (all of size n) rather than an individual void. That is, each discrete element possesses coordinate, n, and weight, ρ. The clusters in a given ensemble are constrained to stay together in size as they evolve, so the particle remains a δ-function in size space, and the particle weight remains constant over time. A particle evolves from size n' to n during a short-time interval, τ, according to the appropriate continuous random walk:

$$n = n' + K(n')\tau + \xi(Q(n'),\tau), \tag{23}$$

using the same drift and diffusion parameters as in the Fokker–Planck short-time propagator approach. This continuous random walk employs a normal deviate, ξ, sampled from the Gaussian distribution, $P(\xi) = \frac{\mathrm{e}^{\xi^2/(2Q\tau)}}{\sqrt{2\pi Q\tau}}$, using the Box–Muller algorithm [21]. The resulting distribution of displacements, $n - n'$, reproduces the short-time propagator on average.

The random-walk of individual particles conserves mass in only the average sense, $\langle \xi_i \rangle = 0$. The overall conservation of mass automatically improves with increasing number of particles; i.e., $\lim_{N\to\infty} \Xi(N) = 0$ for the net error $\Xi(N) = \sum_{i=1}^{N} \rho_i \xi_i$. For practical implementations, it is useful to constrain the random walk so that mass is exactly conserved overall. This requires that $\sum_{i=1}^{N} \rho_i \bar{\xi}_i \equiv 0$ where a correction term is added to each unconstrained ξ_i. To accomplish this, the net error from the unconstrained random walks, Ξ, is distributed among the various particles in proportion to their weight and their RMS deviation:

$$\bar{\xi}_i = \xi_i - \frac{\rho_i\sqrt{Q_i}}{\sum_i \rho_i\sqrt{Q_i}}\,\Xi. \tag{24}$$

This guarantees conservation at all times. The constraint forces the evolution of a single particle to be completely deterministic, but it has little effect on the individual random walks for a large number of particles.

This Fokker–Planck approach is expected to be successful for modeling the distribution of large voids. However, the continuum approximation has difficulties with small-clusters. The requisite assumption of smoothly-varying parameters versus size is no longer valid. Furthermore, in order to employ the short-time propagator, $G(n, n', t)$, the parameters K and Q should be approximately constant over the interval $n - n'$. This implies that τ must be kept small. Finally, Monte Carlo methods are inefficient for studying nucleation from small, unstable clusters. Huge numbers of transitory clusters must be followed in order to identify the few that randomly grow to stable sizes.

Therefore, we split the distribution function into two components, $\rho_{\text{void}} = \rho_{\text{M}} + \rho_{\text{L}}$. The Master equation is used for ρ_{M} with small integer-sized voids, from the vacancy monomer through the (arbitrarily chosen) limit of $N_{\text{M}} = 2000$. The Langevin Monte Carlo method is reserved for ρ_{L}, to describe the larger clusters in continuous size space. The truncated distribution ρ_{M} now obeys the original Dirichlet boundary condition, $\rho_{\text{M}}(1) = C_{\text{v}}$ plus an additional, homogeneous Dirichlet boundary condition at the upper boundary, $\rho_{\text{M}}(N_{\text{M}}) = 0$. Clusters grow to this upper boundary at a rate $\rho_{\text{M}}(N_{\text{M}} - 1)\beta(N_{\text{M}} - 1)$, where they are removed from ρ_{M}. The loss is compensated by creating a new Langevin particle at position $n = N_{\text{M}}$ with amplitude equal to the density of clusters lost, $\rho_{\text{M}}(N_{\text{M}} - 1)\beta(N_{\text{M}} - 1)\tau$. In effect, an artificial sink term in ρ_{M} is paired with an equal source term in ρ_{L}, operating over the time-step, τ.

The Langevin equation allows clusters to evolve to smaller sizes, as well as larger, so the domain for ρ_{L} extends from $n = 1$ to arbitrary size. The boundary condition must be $\rho_{\text{L}}(1) = 0$ in order for the total distribution to satisfy $\rho(1) = C_{\text{v}}$. This constraint is maintained with absorbing boundary conditions – any particle that reaches or crosses the boundary $n = 1$ is deleted from the calculation. Simply applied, this strategy can discard clusters after they shrink to unphysical size, $n < 1$. However, we find that the resulting error is negligible even at the highest temperatures. The error can also be eliminated by using the appropriate restricted Green function near the boundary [10].

In order to preserve numerical accuracy, it is necessary to choose time-steps such that relative changes in ρ_{M} are kept small. The system is initially evolved slowly, to follow the transient development of dimers, trimers, and small-clusters at the outset of the simulation. The time-step is increased exponentially as evolution slows after the initial transient. A maximum value, $\tau_{\max}$, is achieved around the time that C_{v}, C_{i}, and ρ_{M} reach a quasi-stationary limit. The quasi-stationary character permits large numerical time-steps, provided that ρ_{M} is evolved with a numerically stable method. Accordingly, we use the unconditionally stable, backwards Euler method.

In principle, one Langevin particle will be created per time-step, as soon as $\rho_{\text{M}}(N_{\text{M}} - 1)$ achieves a non-zero value. However, this outcome is undesirable in practice, as the computational load will continually increase with time. Particles created at late times may have negligible weight, because $\rho_{\text{M}}(N_{\text{M}} - 1)\beta(N_{\text{M}} - 1)\tau$ is small when the vacancy supersaturation falls to low values. Accordingly, we find it useful to impose a threshold value, ρ_{th}, for the creation of new Langevin particles. If the time-integrated flux of voids at the upper boundary of the Master equation is below this threshold after time-step τ, then the corresponding voids are held at fixed size, N_{M}. Additional voids will accumulate over i successive time-steps until their combined number density $\sum_i \rho_{\text{M}}(N_{\text{M}} - 1, t_i)\beta(N_{\text{M}} - 1, t_i)\tau_i > \rho_{\text{th}}$. All of the accumulated clusters are then transferred to a new Langevin particle, and the process is repeated. Eventually, after void nucleation has largely ceased, the flux of clusters from ρ_{M} is negligible, and no new Langevin elements are created.

The frozen clusters do not contribute to the source/sink terms in the monomer rate equations, because they are fixed in size and therefore prevented from reacting with the monomers. This artificial constraint introduces a cumulative error in the simulated swelling. In order to keep it acceptably small, the frozen clusters should never involve more than a tiny fraction of the total density of voids of similar sizes. Thus, ρ_{th} is a second convergence parameter, besides the maximum time-step value, $\tau_{\max}$. It is typically set at $\rho_{\text{th}} = 10^5\ \text{m}^{-3}$.

2. Results

The mixed Master equation/Fokker–Planck method introduced here is a modification of the path integral Fokker–Planck approach taken by Wehner and Wolfer [10]. The results differ from these early calculations because the model material parameters are slightly changed, the monomer rate equation has been embellished beyond its original form [10,19], and the void cross-sections for vacancy emission have been modified to be consistent with their underlying derivation from a time-reversal argument. In the results reported here, time-steps are chosen so as to maintain conservation of mass at approximately parts in 10^3–10^5 of the steady-state swelling. The absolute conservation is accurate to parts in 10^7 over 40 dpa of fluence. The simulation starts with

$\tau_0 = 10^{-5}$ s in order to follow the transient formation of vacancy dimers, trimers, etc. Time-steps increase successively by 0.1% until $\tau_{max} = 500$ s for irradiation dose rates of 10^{-6} dpa/s. This limit is achieved near 0.5 dpa of fluence, when transient changes to the smaller cluster densities are mostly completed.

The predicted volumetric swelling is easily obtained from the total volume of all voids in the distribution function, neglecting relaxation. Linear dimensions are assumed to increase isotropically, as there is no external stress in these simulations. Fig. 1 shows swelling curves for high-purity austenitic steel, as obtained from the two-component Master/Fokker–Planck method. The 540 °C simulation has a negligibly short rise time to the peak rate of swelling. It reaches a rate of 0.8%/dpa; which subsequently declines slightly. The same material at 600 °C displays a visible swelling delay and reaches a rate of 0.4%/dpa at 100 dpa fluence, where the rate of swelling is still increasing with time. We identify this transient swelling delay with the experimental incubation process. A detailed comparison to experiment will be made in a later publication [22]. Here, it is sufficient to note that experiments on high-purity, ternary Fe–Cr–Ni stainless steels can also show extremely short incubation times for moderate temperatures [23,24]. The observed steady-state swelling rate remains about 1%/dpa. Preliminary calculations with a time-dependent dislocation density appear to give good agreement with experiment [25].

It is useful to examine the corresponding time-dependent void size distributions for the cases of long- and short-incubation times, modeled independently of concurrent dislocation density evolution. Short incubations are characterized by an initially high vacancy supersaturation, which gives very rapid void nucleation. This situation is depicted in Fig. 2, with a series of void size distribution functions at sequential times. The incubation period (defined here as the time to reach the maximum swelling rate) is predicted to last less than 1.0 dpa (≈280 h) in this simulation. The leading edge of the distribution in Fig. 2 advances with time as the largest voids accumulate vacancies. As the total number of voids and average void size increase, the aggregate sink strength for mobile monomer defects also rises, and the vacancy supersaturation decreases. (The monomer vacancy density starts at approximately 6.78×10^{20} m^{-3}, becomes 3.03×10^{20} m^{-3} at 1 dpa, and reaches 1.32×10^{20} m^{-3} by 40 dpa.) As this occurs, the large clusters remain stable and continue to grow. However, small-clusters become increasingly unstable and shrink on average, in a process akin to ripening. A gap opens in the void size distribution, separating the population of small, transient, unstable clusters from the distribution of large, stable voids (cf. Ref. [10]). Critical voids (those at the threshold between stable and unstable sizes) lie near the minimum of the distribution. The height of the distribution function there controls the rate at which new stable voids will nucleate, so the creation of stable voids falls to negligible values as the depression in the distribution progresses.

The data in Fig. 2 are obtained from a pure Master equation approach, using the backwards Euler method. The time-step is set to conserve the total number of atoms to parts in 10^3 of the total swelling. $\tau_{max} = 100$ s by the end of the simulation. Note that practical void

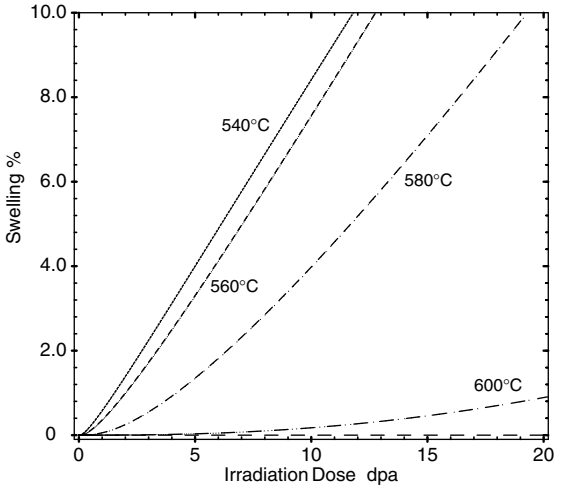

Fig. 1. Swelling curves for type-316 stainless steel with a constant dislocation density of 6×10^{14} m^{-2} at four temperatures.

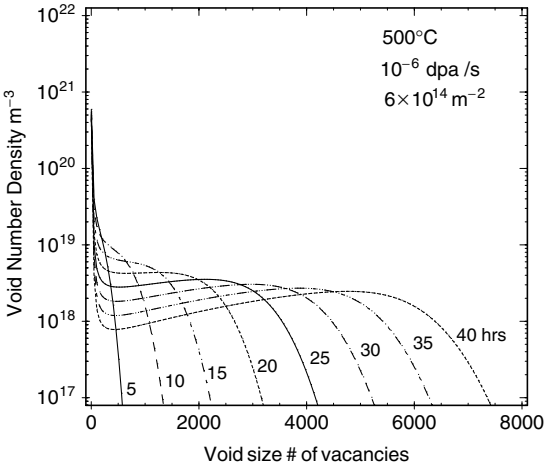

Fig. 2. Void size distribution function versus number of vacancies in the void from a pure Master equation simulation using backwards Euler method for type-316 stainless steel at 500 °C, irradiation dose rate of 10^{-6} dpa/s, and a constant dislocation density of 6×10^{14} m^{-2}. The curves shown correspond to a sequence of instantaneous void size distributions at intervals of 5 h.

swelling simulations may need to reach times of 10^8 s and beyond, so that 10^6 iterations including as many as 10^6 coupled linear equations will be required.

Fig. 3 shows the same distribution function at 40 h, comparing a two-component Master equation/Fokker–Planck treatment to the corresponding pure Master equation results. Small time steps are used to increase the number of Monte Carlo particles and reduce the scatter in the distribution function. The Monte Carlo data has also been partially smoothed by means of a histogram. An additional, least squares fit is made to the histogram using a piecewise linear curve. The fit demonstrates that the Monte Carlo distribution function is equivalent to the solution of the full Master equation. At $t = 40$ h (0.144 dpa), approximately 1700 Langevin particles have been formed. The maximum number of particles ($\approx$12 000) is reached near 1.2 dpa. The asymptotic number is only $\approx$9500, because some of the particles shrink and are eventually deleted from the simulation. At the peak rate of formation, particles are created at every time-step with weights on the order of 10^{19} m^{-3}.

For this 500 °C calculation, the initial, transient behavior involves the pinching off of the distribution of large, stable clusters from the narrow peak of small, unstable clusters (Fig. 2). When the separation is more complete, the small-cluster distribution ρ_M is quasi-stationary, and its evolution is controlled by the rate at which the large clusters grow. The stable clusters in ρ_L grow larger with time, shifting the upper bulge in the distribution to larger sizes while changing its shape only gradually. In most calculations at 10^{-6} dpa/s, $\tau_{max} = 500$ s, typically 10^3–10^5 Langevin particles are introduced.

Ideally, the two-part distribution function assigns all unstable clusters to the Master equation treatment, while the stable voids are modeled with the Langevin Monte Carlo scheme. In that case, the Master equation cutoff, N_M, would be chosen to lie at or above the critical void size. This is the case at 500 °C, but it is not practical at high temperatures or low dose-rates, where the stable void size may be very large. The distribution function for a high temperature case (at 600 °C) is shown in Fig. 4. Here, stable voids nucleate much more slowly from the low initial vacancy supersaturation. Even after extended periods of void nucleation, the accumulated voids contribute negligible amounts to the monomer sink strength, as compared to the (constant-density) dislocations. Therefore, the monomer rate equations are essentially invariant over the period displayed in Fig. 4, and the vacancy supersaturation remains almost constant with time. (The vacancy concentration is 1.04×10^{20} m^{-3} at the outset, 1.03×10^{20} m^{-3} at 10 dpa, and 9.63×10^{19} m^{-3} at 50 dpa.) By similar reasoning, the net dimer formation rate ($v + v \Longleftrightarrow v_2$ and $v_2 + i \rightarrow v$ reactions) and the dimer density obtain a quasi-stationary limit, after the initial transient when dimers are formed. In this quasi-stationary limit, a constant net number of dimers are created from monomers per unit time, but almost equal numbers grow to become trimers. This same argument applies to successively larger voids until the leading edge of the void size distribution is reached, where there is a transient increase in the

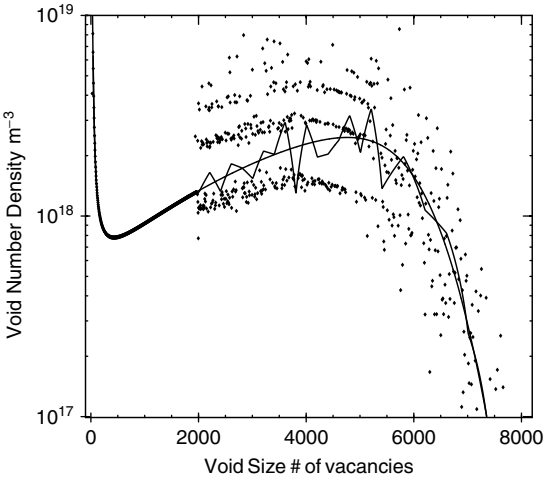

Fig. 3. A comparison of the Master equation solution to the two-component Master/Fokker–Planck results with the same $\tau_{max} = 100$ s, at $t = 40$ h and 500 °C. The pure Master equation solution is shown with a smooth, solid line. The scatter-plot shows a histogram of the raw Monte Carlo simulation. A piecewise linear fit to the histogram is shown with a jagged solid line.

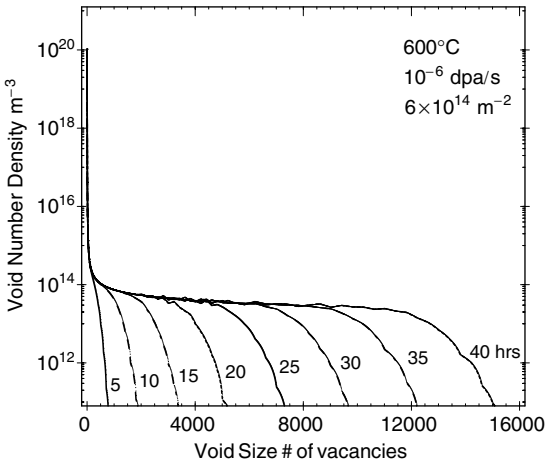

Fig. 4. Void size distribution function versus number of vacancies in the void. Distributions are shown for every 5 h of exposure, up to 40 h. This simulation corresponds to a temperature of 600 °C, dose rate of 10^{-6} dpa/s, and dislocation density of 6×10^{14} m^{-2}. Here, $\tau_{max} = 5$ s is chosen so as to reduce the statistical noise (cf. Fig. 3).

distribution function. The net effect is that the distribution function only increases at the advancing upper end of the distribution function. As time progresses, the leading edge moves to larger sizes, and yet larger voids approach a quasi-stationary distribution. Eventually, the void sink strength will increase to significant levels, vacancy supersaturation falls, and further void nucleation ceases. However, in this case, nucleation and incubation are unfinished even at 100 dpa.

Figs. 2 and 4 serve to illustrate an important adiabatic principle in the evolution of the overall distribution. Individual small-clusters undergo especially rapid evolution, randomly losing vacancies at a high rate while only occasionally absorbing a vacancy. They are unstable and tend to disappear, on average. Their rapid evolution makes for stiff rate equations governing the distribution of small-clusters. It also implies that the small-cluster distribution will rapidly adjust to and subsequently closely track any slow changes in the system parameters. As a result, the relevant time-scale for the evolution of small-void densities is dictated by the overall evolution of the system, not by the characteristic rates of reaction of the small-clusters with the mobile defects. Separating out the small-cluster ρ_M and imposing time-independent boundary conditions on the upper end allows it to reach a quasi-stationary limit, permitting the use of larger time-steps. This same principle motivates the quasi-stationary approximation in the monomer rate equations.

3. Conclusion

We present a numerical scheme to treat void nucleation and growth on the same footing. Our new implementation is able to account for transient behavior yet remain efficient at long times. We have applied it to pure type-316 stainless steels, looking at void evolution only – all other aspects of the microstructure are held fixed at this time. We observe separate incubation and swelling regimes. Our results lack the substantial incubation period of commercial steels except at high T. High-purity steels, on the other hand, can have very short incubation times, in better agreement with the predictions of the present simulations [23,24]. We see clear indications that incubation and void nucleation are related, although they are not synonymous. Small vacancy clusters/voids form and disappear continually, maintaining an appreciable population of sub-critical clusters as long as radiation damage persists. Initially, this sub-critical population provides a small flux of voids to form a more permanent population of larger voids (i.e. nucleation of stable voids). During the incubation period, void swelling is determined by both this influx as well as the continued growth of permanent voids. As the stable population increases, the influx from the sub-critical population diminishes. Eventually, the influx effectively ceases, and the permanent voids reach their maximum growth rate, as steady-state swelling is attained. Nevertheless, there remains a sub-critical vacancy cluster and void population that changes only slowly in response to the increase in the densities of both permanent voids and dislocations. This sub-critical void population contributes a competing sink for vacancies and interstitials; it has become a population of persistent recombination sites. Realistic simulations of transient irradiation swelling need to include all of these effects.

Void nucleation proceeds in this model despite the lack of helium or other gas impurities and in the absence of any production bias. This may result from our neglect of vacancy loop nucleation and formation of stacking fault tetrahedra in competition with the formation of three-dimensional vacancy clusters. In any case, however, our simulations show that any supersaturation of vacancies will create stable voids at a non-zero rate, however small.

This paper is intended primarily to develop and introduce a novel approach to the non-equilibrium evolution of a cluster population. At this time, it is only applied to a void population growing from mobile monomers. Thus, the model does not allow for loop nucleation and growth and does not account for 'production bias' of preformed defect clusters from large damage cascades [26]. Suitable generalizations of this new method will be suited to the evolution of other clusters, including bubbles and dislocation loops. Because the time-dependence of the total system is governed by a complex co-evolution all of its constituents, we plan to successively incorporate additional features in the model. This incremental approach will better expose the relative importance of different cluster species and reaction processes. It will similarly reveal the nature of their mutual interactions and the effect of their interactions on swelling behavior.

Acknowledgements

This work was performed under the auspices of the US Department of Energy by the University of California, Lawrence Livermore National Laboratory under contract no. W-7405-Eng-48. This research was funded by the Department of Energy's Nuclear Energy Research Initiative (NERI) Program through the Office of Nuclear Energy, Science, and Technology.

References

[1] F.A. Garner, J. Nucl. Mater. 122&123 (1984) 459.
[2] F.A. Garner, J. Nucl. Mater. 205 (1993) 98.
[3] F.A. Garner, M.B. Toloczko, J. Nucl. Mater. 206 (1993) 230.

[4] F.A. Garner, M.B. Toloczko, B.H. Sencer, J. Nucl. Mater. 276 (2000) 123.
[5] T. Okita, T. Kamada, N. Sekimura, J. Nucl. Mater. 283–287 (2000) 220.
[6] W.G. Wolfer, A. Si-Ahmed, Philos. Mag. A 46 (1982) 723.
[7] A.D. Brailsford, R. Bullough, J. Nucl. Mater. 44 (1972) 121.
[8] B.B. Glasgow, A. Si-Ahmed, W.G. Wolfer, F.A. Garner, J. Nucl. Mater. 103 (1981) 981.
[9] K.C. Russell, Acta Metal. 26 (1978) 1615.
[10] M.F. Wehner, W.G. Wolfer, Philos. Mag. A 52 (1985) 189.
[11] A.V. Barashev, D.J. Bacon, S.I. Golubov, J. Nucl. Mater. 276 (2000) 243.
[12] R. Bullough, B.L. Eyre, K. Krishnan, Proceedings of the Royal Society of London A vol. 346 (1975) 81.
[13] Y. Katoh, T. Muroga, A. Kohyama, R.E. Stoller, C. Namba, J. Nucl. Mater. 233–237 (1996) 1022.
[14] A.A. Semenov, C.H. Woo, J. Nucl. Mater. 205 (1993) 74.
[15] C.H. Woo, B.N. Singh, Phys. Stat. Sol. B 159 (1990) 609.
[16] C.H. Woo, B.N. Singh, Philos. Mag. A 65 (1992) 880.
[17] J.J. Sniegowski, W.G. Wolfer, in: J.W. Davis, D.J. Michel (Eds.), Proceedings of Topical Conference on Ferritic Alloys for use in Nuclear Energy Technologies, Snowbird, Utah, 1983, p. 579.
[18] W.G. Wolfer, M.H. Yoo, in: J.S. Watson, F.W. Wiffen (Eds.), International Conference on Radiation Effects and Tritium Technology for Fusion Reactors, vol. 2, Gatlinburg, Tennessee, 1976, p. 458.
[19] W.G. Wolfer, B.B. Glasgow, Acta Metal. 33 (1985) 1997.
[20] L.G. Shampine, C.W. Gear, SIAM Rev. 21 (1979) 1.
[21] W.H. Press, S.A. Teukolsky, W.T. Vetterling, B.P. Flannery, Cambridge University, New York, 1992.
[22] M.P. Surh, J.B. Sturgeon, W.G. Wolfer, submitted.
[23] T. Okita, Doctoral thesis, University of Tokyo, University of Tokyo, 2001.
[24] T. Okita, T. Sato, N. Sekimura, F.A. Garner, L.R. Greenwood, J. Nucl. Mater. 307–311 (2002) 322.
[25] M.P. Surh, J.B. Sturgeon, W.G. Wolfer, in: M.L. Grossbeck, T.R. Allen, R.G. Lott, A.S. Kumar (Eds.), Effects of Radiation on Materials: 21st International Symposium, ASTM STP, 1447, ASTM International, West Conshohocken, PA, 2003.
[26] H. Trinkaus, B.N. Singh, J. Nuc. Mater. 307–311 (2002) 900.